Supporting information for: X-Ray Imaging of Functional Three-Dimensional Nanostructures on Massive Substrates

Diana A. Grishina,[†,¶] Cornelis A. M. Harteveld,[†] Alexandra Pacureanu,[‡] D. Devashish,[†,§] Ad Lagendijk,[†] Peter Cloetens,[*,‡] and Willem L. Vos[*,†]

[†]*Complex Photonic Systems (COPS), MESA+ Institute for Nanotechnology, University of Twente, P.O. Box 217, 7500 AE Enschede, The Netherlands*

[‡]*ESRF-The European Synchrotron, CS40220, 38043 Grenoble, France*

[¶]*Current address: ASML Netherlands BV Building 21, de Run 1, Veldhoven, North Brabant, NL 5504 DR, The Netherlands*

[§]*Current address: ASML Netherlands B.V., 5504 DR Veldhoven, The Netherlands*

E-mail: cloetens@esrf.eu; w.l.vos@utwente.nl

Supporting Information Available

This supplementary features details of the CMOS compatibility of TXT, the reflectivity setup, details of the theory, features of the reconstructed crystals, and video animations.

1 CMOS Compatibility of TXT

The TXT technique is not limited to silicon based structures, not limited to specific sample geometries, and TXT works on both non-periodic and periodic samples. Basically there

should be sufficient transmitted X-rays, and the material contrast should be sufficiently high, and features should be spatially resolvable, as is discussed in the Methods.

The transmission should be high enough to preserve good photon statistics and avoid artefacts, hence a transmission $T > 10\%$ is typically preferred. For silicon, this corresponds at the 17 keV photon energy used in TXT to 1.5 mm thick wafers, much thicker than standard CMOS wafers. In contrast, with previous X-ray methods at 6 or 8 keV only 70 to 150 microns of Si can be traversed, therefore samples have to be thinned down.

The material contrast is determined by the density difference between the materials that need to be distinguished. The required density difference of a few 0.01 g/cm^3 is easily reached for different typical CMOS materials. For instance, the density difference between silicon and aluminum is $\Delta\rho = 0.37$ g/cm^3 and between silicon and photoresist (SU-8) $\Delta\rho > 1$ g/cm^3. The effective density resolution will however strongly depend on the 'dynamic range' of the sample (it is much more difficult to resolve minute density changes in close proximity to huge ones) and should be considered on a case by case basis.

2 The Optical Reflectivity Setup

The main components of the reflectivity setup are a supercontinuum white light source (Fianium), a Fourier-transform interferometer (Biorad FTS-6000) that operates with 8 cm^{-1} spectral resolution, and a reflecting objective $NA = 0.65$ to focus the beam to a few microns inside the photonic crystal domains over the large required range of frequencies. Signals were collected in the near infrared spectral range between about 4000 cm^{-1} and more than 12500 cm^{-1}, corresponding to wavelengths between 2500 and 800 nm. Reflectivity was calibrated by taking the ratio of a sample spectrum with the spectrum measured on a clean gold mirror. In the spectra in Figs. 2B,D,F a narrow range near 9300 cm^{-1} is omitted since it is disturbed by the pump laser of the supercontinuum source (Fianium). The maximum

reflectivity in Fig. 2B is limited to 45% due to several different reasons: the white light focus has a diameter of about 4 μm that is comparable to the extent over which the crystal is homogeneous; near the crystal-air interface the pores reveal roughness as a result of the etching process, so-called "scallops".[S1,S2]

3 Photonic Crystal Theory

Photonic band structures, in other words, the fundamentally important dispersion relations between the frequency and the wave vectors of the crystal Bloch modes,[S3,S4] were calculated with the plane-wave expansion method, using the MIT photonic bands (MPB) code.[S5] In the plane-wave expansion method, the unit cell of the crystals was discretized with a high spatial resolution $(\Delta X, \Delta Y, \Delta Z) = (c/140, a/200, c/140)$. The band structures are represented as reduced frequency a/λ versus reduced wave vector ka between high-symmetry points (R, Y, S, R, T, Y, Γ, X, U, Γ, Z, U, R) in the 1st Brillouin zone of the convenient tetragonal representation of the unit cell.[S4,S6] The assignment of the polarization states of the photonic bands that bound the $\Gamma - X$ stop gap (or symmetrically equivalently the $\Gamma - Z$ gap; see Fig. 1B) is based on our recent computational study.[S7] The photonic bands in Figure 1B and the gap in Fig. 2B were calculated for a relative pore radius $r/a = 0.267$ as borne out of the X-ray tomography data, and the gaps in Figs. 2D,F were calculated for the designed pore radius $r/a = 0.245$.

4 The Reconstructed Crystal

A salient feature in Figure 3B is that the pores running in the X-direction are not exactly perpendicular to the pores in the Z-direction. It appears that the angle between the pore arrays deviates from the 90^o design by $\Delta\alpha = 2^o$; from results on several crystals we find

deviations between $\Delta\alpha = 0^o$ and 6^o. We attribute the slight variations to the limited precision in placing a sample in the etching chamber during nanofabrication. From separate plane-wave band structure calculations we find that the 3D photonic band gap is robust and remains very broad, as the relative bandwidth changes from $\Delta\omega/\omega_c = 0.24$ to $\Delta\omega/\omega_c = 0.21$ in case of a slight $\Delta\alpha = 5^o$ shear of the cubic crystal structure.[S8]

The estimated X-ray skin dose has an upper limit (neglecting the attenuation by the Si substrate) of about 3.10^8 Gy for the Good and Bad samples and 9.10^8 Gy for the Ugly sample, which is expected to have little effect on Si nanostructures that are placed in a high vacuum during the experiments.

5 Multimedia Files

In view of the richness of the 3D reconstructions, we provide here movie animations of rotations about and cross-sections through the 3D data volumes.

S1 Animation 'theGood.avi': Colour animation of a rotation of the successfully etched "Good" crystal shown in Fig. 3A-B about the vertical axis in Fig.3 A. The animation shows the reconstructed sample volume from all viewing directions. Still at 0:01 is shown below.

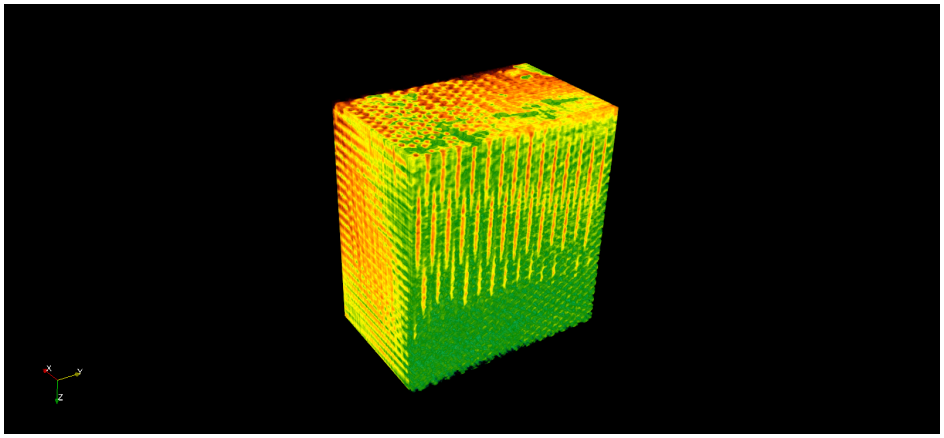

S2 Animation '*S2_theGood2_2019_small*.avi': Black and white animation of YZ cross-sections scanned in the X-direction through the successfully etched "Good" crystal shown in Fig. 3A-B, resampled to 5 MB file size. Still at 0:04 is shown below (white structures are dust particles).

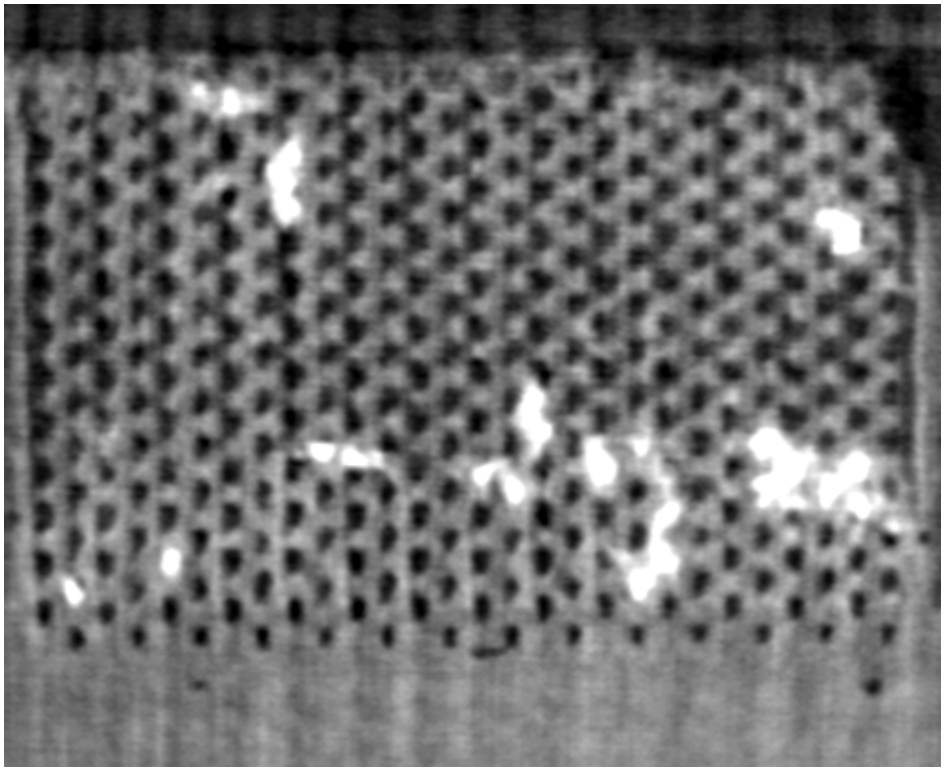

S3 Animation '*S3_theGood2_2019_sec3-19*.avi': High resolution version of the previous movie cropped to a short range near the "Good" crystal surface. Still at 0:08 is shown below.

S4 Animation '*S4_theBad_2019_small*.avi': Black and white animation of YZ cross-sections scanned in the X-direction through the crystal with a void ("the Bad") shown in Fig. 3C-D, resampled to 5 MB file size. The scan starts from the substrate, scans parallel to X-oriented pores, traverses the stiction-induced void (where the surrounding 2D photonic crystal pores are still apparent left and right), and finishes in air above the crystal surface. Still at 0:08 is shown below.

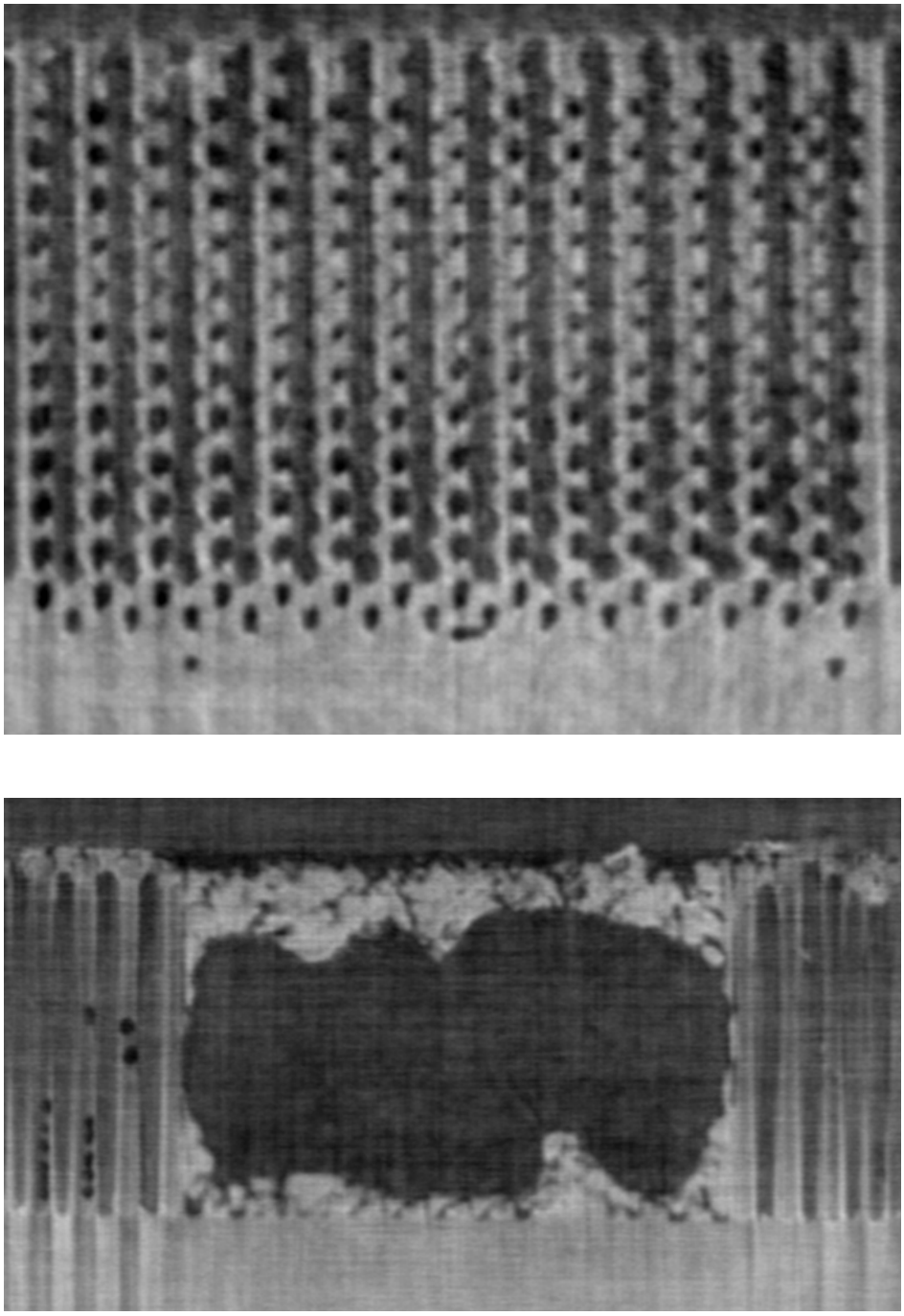

S5 Animation '*S5_theUgly_*2019.avi': Black and white animation of YZ cross-sections scanned in the X-direction through the erroneously etched structure similar to Fig. 3E-F. The scan starts just outside the external surface (showing a dust particle on the surface), and scans parallel to X-oriented pores into the bulk silicon, while at the top

the shallow pores in the Z-direction are seen. At the left, a second nanostructure is seen. Still at 0:02 is shown below.

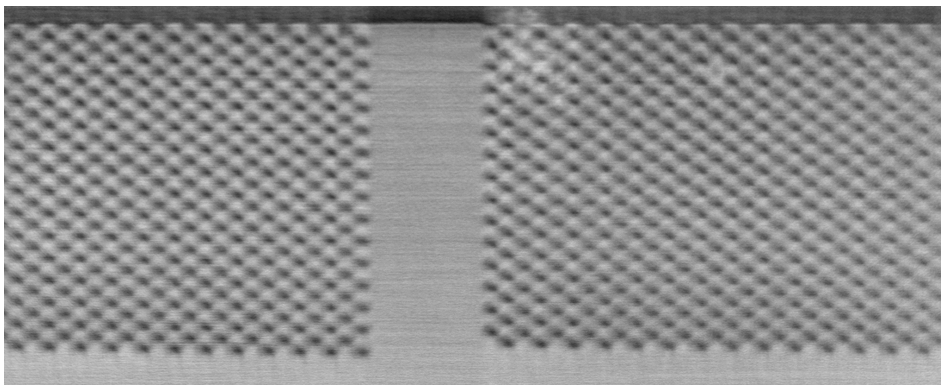

References

(S1) Wu, B.; Kumar, A.; Pamarthy, S. High Aspect Ratio Silicon Etch: A Review. *J. Appl. Phys.*, **2010**, *108*, 051101:1-20.

(S2) van den Broek, J. M.; Woldering, L. A.; Tjerkstra, R. W.; Segerink, F. B.; Setija, I. D.; Vos, W. L. Inverse-Woodpile Photonic Band Gap Crystals with a Cubic Diamond-Like Structure Made from Single-Crystalline Silicon. *Adv. Func. Mat.*, **2012**, *22*, 25-31.

(S3) Ashcroft, N. W.; Mermin, N. D. *Solid State Physics*. Holt, Rinehart, and Winston: New York, 1976.

(S4) Joannopoulos, J.D; Johnson, S.G.; Winn, J.N.; Meade, R.D. *Photonic Crystals: Molding the Flow of Light*. Princeton University Press: Princeton, 2008.

(S5) Johnson, S.G.; Joannopoulos, J.D. Block-iterative Frequency-Domain Methods for Maxwells Equations in a Planewave Basis. *Opt. Express* **2001**, *8*, 173-190.

(S6) Huisman, S.R.; Nair, R.V.; Woldering, L.A.; Leistikow, M.D.; Mosk, A.P; Vos, W.L

Signature of a Three-Dimensional Photonic Band Gap Observed with Silicon Inverse Woodpile Photonic Crystals. *Phys. Rev. B* **2011**, *83*, 205313: 1-7.

(S7) Devashish, D.; Hasan, S. B.; van der Vegt, J. J. W.; Vos, W. L. Reflectivity Calculated for a Three-Dimensional Silicon Photonic Band Gap Crystal with Finite Support. *Phys. Rev. B* **2017**, *95*, 155141: 1-12.

(S8) Woldering, L. A.; Mosk, A. P.; Tjerkstra, R. W.; Vos, W. L. The Influence of Fabrication Deviations on the Photonic Band Gap of Three-Dimensional Inverse Woodpile Nanostructures. *J. Appl. Phys.* **2009**, *105*, 093108: 1-10.